

DesignCon 2016

PCB-Substrate Characterization at Multigigahertz Frequencies Through SIW Measurements

Gabriela Méndez-Jerónimo, INAOE

Svetlana C. Sejas-García~
Chudy Nwachukwu
Isola

Reydezel Torres-Torres, INAOE

Abstract

Substrate integrated waveguides (SIWs) mimic the behavior of rectangular waveguides (RWGs) and can be implemented with standard PCB technology. In fact, when the diameter and the spacing between the plated-through holes forming the sidewalls is much smaller than the wavelength of the signals launched into the SIW, the theory used to analyze RWGs can be applied to analyze the electrical properties of these structures. Therefore, it is reasonable to assume that a SIW maintains the electromagnetic (EM) fields confined within its structure much like a RWG. This implies that the properties of the materials forming these waveguides can be obtained from S-parameter measurements. Moreover, since most of the energy is guided through the dielectric, the metal losses are substantially lower than in conventional microstrip and stripline-based test vehicles used for characterization purposes. Actually, full-wave simulations and experimental data presented here verify this fact at microwave frequencies. Thus, SIWs are candidates for implementing prototypes to characterize dielectrics at frequencies within the capacity of vector network analyzers available in most microwave laboratories.

Previous proposals have taken advantage of the properties of the SIWs to characterize PCB dielectrics, but in order to keep the analysis simple, the effect of the metal losses are typically neglected. Even though these losses are significantly smaller than those associated with the dielectric, significant overestimation can be introduced in the determined dissipation factor when the effect of the currents flowing through the metallization is ignored. Other approaches account for dielectric and metal losses, but parameter optimization is applied to correlate simulated and experimental curves, which may yield unphysical results to the obtained figures of merit. Alternatively, resonators based on SIWs can be implemented to reduce the uncertainty of the model-experiment correlations. In this case, however, the bandwidth of the parameter extraction is very limited.

To overcome the disadvantages of previously reported approaches, a systematic and analytical parameter extraction methodology to obtain the frequency dependent permittivity (Dk) and loss tangent (Df) at tens of gigahertz and within a wide band (also of tens of gigahertz) is proposed here. These data can either be used for material assessment or for interconnect modeling considering the corresponding structure.

The proposed methodology is based on the experimental determination of the propagation constant. For this purpose, different signal launches are used to observe the optimal transition to excite the SIW within a given frequency band. Afterwards, the data corresponding to the total attenuation is processed so that data regressions can be used to obtain the associated parameters without neglecting any significant contribution. Moreover, SIWs with different widths and heights are used to systematically analyze the impact of scaling their size on the corresponding losses. This provides insight about the advantages and disadvantages of narrowing the SIW to extend the frequency at which Dk and Df can be obtained. In this regard, the importance of processing data corresponding to higher order modes propagated in the SIW instead of shrinking its size is also illustrated.

Authors Biography

Gabriela Méndez-Jerónimo was born in Veracruz, Mexico. She received the B.S. degree in Electronics from the Instituto Tecnológico de San Luis Potosí, SLP, in 2012 and the M.S. degree in the National Institute for Astrophysics, Optics and Electronics (INAOE), Puebla, Mexico, in 2014 where she is currently working toward the Ph.D. degree in Electronics. Her areas of interest include high-frequency measurement, characterization, and modeling of PCB materials and interconnects for high-speed applications.

Svetlana C. Sejas-García is an engineer in Isola's R&D team. She was born in Puebla, Mexico. She received the B.S. degree in Electronics from the Benemérita Universidad Autónoma de Puebla, Puebla, in 2005 and the M.S. degree in electronics from INAOE, Puebla, in 2009. She received the Ph.D. degree in electronics from INAOE, Puebla, in 2014 by researching the effects occurring in complex chip-to-chip communication channels and passive components. In 2008, she was an Intern with Intel Laboratories, Mexico, working on the development of models for high-speed interconnects.

Chudy Nwachukwu manages the Signal Integrity Laboratory and SaaS Application Development for Isola USA Corp. located in Chandler, Arizona. His previous work experiences with Force10 Networks and Gold Circuit Electronics included but were not limited to: PCB interconnect design, project management, research and development, and technical sales/marketing. Chudy received his MBA degree from Arizona State University, and M.S.E.E. degree from Saint Cloud State University. He graduated with a Bachelor's degree in Mathematics and Computer Science from Southwest Minnesota State University in Minnesota.

Reydezel Torres-Torres is a senior researcher in the Electronics Department of INAOE in Mexico. He has authored more than 60 journal and conference papers and directed several Ph.D. and M.S. theses, all in experimental high-frequency characterization and modeling of materials, interconnects, and devices for microwave applications. He received his Ph.D. from INAOE and has worked for Intel Laboratories in Mexico and IMEC in Belgium.

1 Introduction

Characterizing the dielectric properties of materials is one of the main topics studied in R&D laboratories of the PCB industry. This is due to the fact that the interaction of EM waves with the dielectric environment surrounding the PCB interconnects yields loss of power and delay. In fact, this is especially important at multi-gigahertz frequencies at which the dielectric losses significantly contribute to the total signal attenuation. Thus, accurate characterization techniques and methodologies allow material engineers to get insight about the properties of a given material during its development, but also provide information to the circuit designer on how to implement reliable circuit models when designing a product.

Thus, many methodologies and hundreds of papers have been published reporting a wide variety of methods for determining the dielectric constant (Dk) and dissipation factor (Df) of the dielectric materials [1]. These methods can be grouped into different categories in accordance to the test structure used to experimentally obtain the dielectric properties; three of the most widely used are those employing: resonators, transmission lines, and capacitors. A brief description of the main advantages and disadvantages of these methods are summarized in Table 1.

With the advent of new PCB fabrication process technologies, it has been possible to manufacture materials with ultra-low losses when compared with traditional FR4 laminates. Evidently, the application of these advanced materials is intended for high-speed applications where data transfer rates beyond 20+ Gbps required. In this case, knowledge of the characteristics of the dielectric at tens of gigahertz is needed within a wide range of frequencies. As can be seen in Table 1, however, current techniques

	Resonators	Transmission lines (microstrips and striplines).	Capacitors
Advantages	<ul style="list-style-type: none"> * Accurate extraction of Dk and Df at microwave frequencies. 	<ul style="list-style-type: none"> * Easy implementation of prototypes. * Broadband. 	<ul style="list-style-type: none"> * Quick and simple measurements.
Disadvantages	<ul style="list-style-type: none"> * Results for a single point of frequency (i.e. the dimensions of the resonator determines the frequency of application). * A sample for calibration is required [2]. * Many structures are required to obtain dielectric properties within a wide frequency range [3]. 	<ul style="list-style-type: none"> * Accurate determination of frequency-dependent characteristic impedance is required (not easy due to the effect of signal launchers). * Dependent on PCB stack-up (e.g., the dielectric on top of a stripline is not exactly the same as that on bottom). 	<ul style="list-style-type: none"> * Accuracy is affected by air gaps. * Limited in frequency due to test fixture parasitics.

Table 1: Brief review for some of the most used methods for characterizing dielectrics.

present limitations to carry out this task; thus, a combination of methodologies to perform parameter extractions at the frequencies of interest are commonly applied. For instance, focusing on transmission line-based techniques, which theoretically allow for the determination of Dk and Df at the frequencies at which S-parameter measurements are performed, one of the main drawbacks is the considerable signal attenuation at frequencies of tens of gigahertz for current technologies. This is mainly due to the significant conductor losses associated with the finite conductance of the metal traces, an effect that is accentuated as the width of the interconnects is reduced to achieve 50Ω of impedance in advanced thin dielectric substrates. Moreover, additional effects such as that related with the filling factor in microstrip lines and considerable vertical parasitics to access striplines make difficult the accurate characterization of dielectrics.

Alternatively, appropriately designed rectangular waveguides (RWGs) can be used as characterization test vehicles at frequencies of tens of gigahertz because they present substantially less conductor losses than conventional quasi-TEM transmission lines (e.g., striplines and microstrip lines). Fortunately, this kind of structure can be easily emulated using the substrate-integrated-waveguide (SIW) concept [4, 5]. Thus, a SIW can be implemented on PCB, allowing to accurately obtain the characteristics of the dielectric enclosed by the conductor boundaries of its structure. In fact, this is the topic of study in this paper; Dk and Df are determined here as function of frequency using simple but rigorous waveguide theory. Furthermore, the analysis presented here also allows to experimentally identifying the variation of the attenuation characteristics of a SIW with geometry. This provides insight about the optimal dimensions of the test vehicle for application within a certain frequency range.

Description of a SIW

A SIW was formerly known as ‘synthetic rectangular waveguide’ since it is a structure fabricated in PCB technology which mimics the behavior of a RWG. Fig. 1 shows a simplified sketch illustrating the geometry of a SIW. As can be seen, it consists of two parallel metal plates (top and bottom) separated by a dielectric substrate with thickness t and two side walls formed by metal vias.

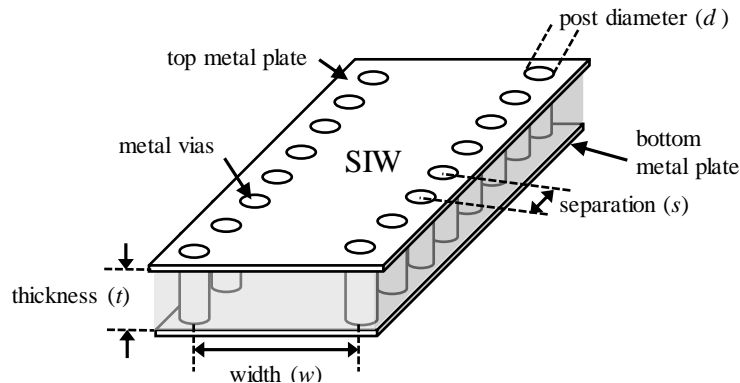


Figure 1: Sketch of a substrate integrated waveguide (SIW) detailing its dimensions.

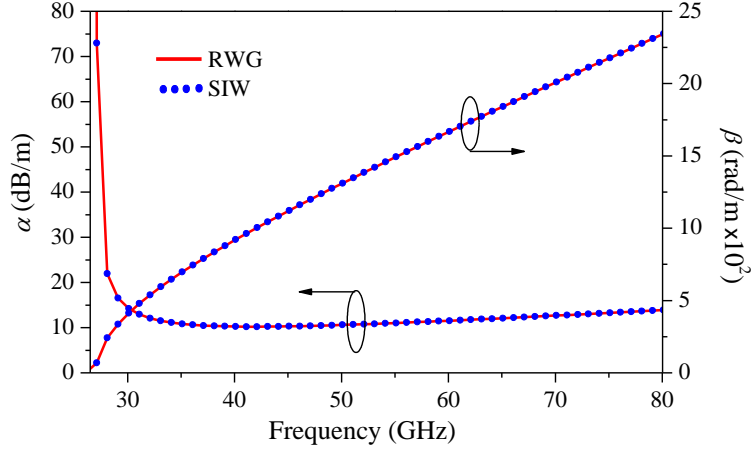


Figure 2: Comparison between the propagation constant [real (α) and imaginary (β) parts] obtained from full-wave simulations of RWG and SIW structures.

Notice in Fig. 1 that a SIW is not a perfect RWG since the side walls are formed with closely spaced metallic posts (e.g. vias) instead of solid metallic planes. Nonetheless, if the wavelength (λ) of the highest frequency harmonic of the signal propagated through the SIW is large when compared to the distance between the posts, then the leakage of energy through the synthetic walls is small. In this case, for practical purposes the SIW can be accurately represented using RWG theory. More specifically, according to [6, 7], for this assumption to be valid the diameter (d) and the maximum separation (s) of the posts are respectively defined as:

$$d < \frac{\lambda_g}{5} \quad (1)$$

$$s < 2d \quad (2)$$

Where λ_g is the smallest wavelength of a signal component traveling through the SIW. At this point, it is also necessary to mention that the effective width of the SIW can be obtained from [8, 9]:

$$w_{eff} = w - \frac{d^2}{0.95s} \quad (3)$$

which means that the SIW can be treated as a RWG presenting a width w_{eff} . Bear in mind that (3) is only valid when conditions (1) and (2) are met [10].

Now, it is well known that a SIW behaves like a high-pass filter with a cutoff frequency that can be calculated based on its geometry and dielectric properties. Assuming that the TE_{10} fundamental mode is excited through a stimulus at the middle of the SIW width, the corresponding cutoff frequency for this mode can be calculated as:

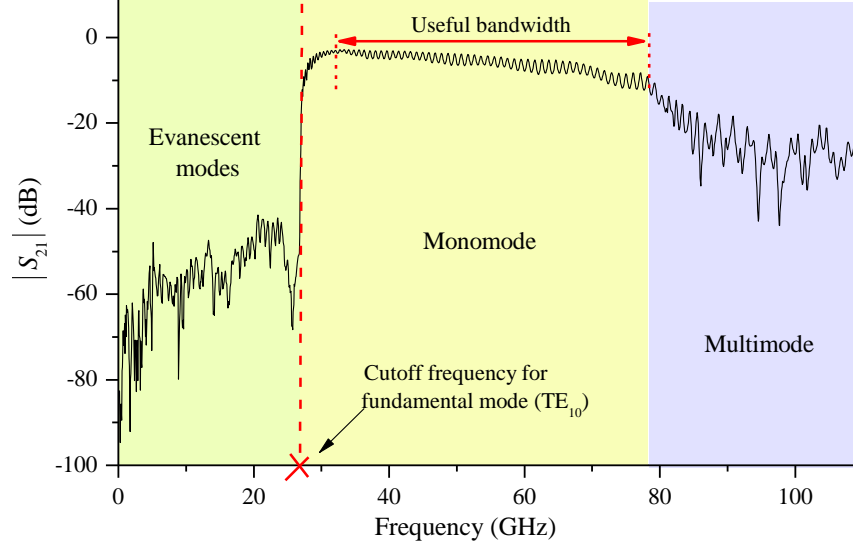


Figure 3: Experimental insertion loss for a SIW designed to operate in the TE_{10} mode.

$$f_c = \frac{c}{2w_{eff}\sqrt{\epsilon_r}} \quad (4)$$

For the sake of illustrating how accurately the behavior of a RWG is emulated by a SIW, full-wave simulations of one structure of each kind were performed considering equivalent widths and the same material properties. This means that both structures were designed to present the same cutoff frequency (27 GHz). Fig. 2 shows the confrontation of the simulated results for the complex propagation constant obtained in both cases, which points out the fact that the SIW can be seen as a RWG.

Regarding the implementation of SIWs as test vehicles for dielectric material characterization, the useful bandwidth is determined based on the frequency range where single mode propagation occurs. This is defined from the cutoff frequency of the fundamental mode up to the cutoff frequency of the first higher order mode excited in the guide. However, due to the high attenuation at frequencies slightly above the cutoff frequency, an empirical criterion defines the lower limit of the bandwidth of operation as $1.25 f_c$ [11]. Fig. 3 details the frequency ranges corresponding to the different operation regions for a SIW. The reason why single mode propagation is preferred versus multimode propagation is because of two facts: it is much simpler to process data corresponding to only one mode of propagation, and the applied power is not split between modes (which would reduce the signal-to-noise ratio for each mode).

Another aspect that should be considered when selecting SIWs over quasi-TEM transmission lines for dielectric characterization is the attenuation suffered by the signal at the frequencies of interest. Fig. 4 shows that this attenuation is considerably smaller for a SIW operated in the monomode region than for the case of a stripline with a similar cross section. In fact, this is one of the reasons why SIWs are good candidates to perform PCB material characterization at tens of gigahertz.

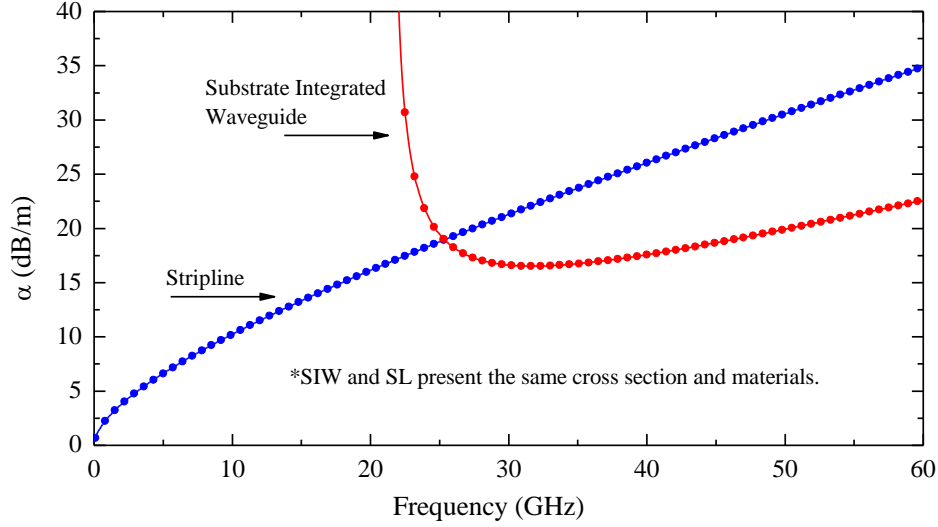


Figure 4: Comparison between the attenuation obtained from full-wave simulations of a SIW and stripline with similar cross section of a SIW.

2 Quantification of Losses through Full-Wave Simulations

The total attenuation that a signal suffers while traveling along a SIW within the frequency range of operation is approximately the result of the dielectric and conductor losses. Thus, the attenuation can be expressed as:

$$\alpha_{total} = \alpha_d + \alpha_c \quad (5)$$

where α_d and α_c represent the contributions of the dielectric and conductor losses, respectively. Thus, when characterizing the losses associated with the dielectric substrate where the SIW is formed, α_d must be obtained from the experimentally obtained α_{total} . Hence, quantifying the contribution of each type of loss in the total attenuation is necessary. For this purpose, modeling the loss mechanisms occurring in a SIW based on RWG theory can be applied. This methodology is shown in greater detail later in this paper.

Dielectric Losses

The electric properties of dielectric media are analyzed using a representation of electric dipoles. Thus, when EM waves travel through dielectric materials, the time-varying fields make these dipoles oscillate causing that part of the EM energy is absorbed by the material, which results in signal attenuation. In order to evaluate this effect, the so-called dissipation factor (Df) is defined (also known as the loss tangent), which is mathematically expressed as:

$$Df = \frac{\epsilon_i}{\epsilon_r} \quad (6)$$

where ε_r and ε_i represent the real and imaginary parts of the complex relative permittivity, respectively given by [12]:

$$\varepsilon_r = Dk = \frac{\beta^2 + \left(\frac{\pi}{w_{eff}}\right)^2}{(2\pi f)^2 \mu_0 \varepsilon_0} \quad (7)$$

$$\varepsilon_i = \frac{\alpha_d \varepsilon_r}{\pi f \sqrt{\mu_0 \varepsilon_0 \varepsilon_r}} \sqrt{1 - \left(\frac{1}{w_{eff} 2f \sqrt{\mu_0 \varepsilon_0 \varepsilon_r}}\right)^2} \quad (8)$$

where w_{eff} was defined in (3), and μ_0 and ε_0 are the free-space permeability and permittivity, respectively.

In this case, according to [13], the attenuation due to the dielectric (α_d) can be represented by means of:

$$\alpha_d = \frac{k_1}{\beta} f^2 \quad (9)$$

where

$$k_1 = 2\pi^2 \mu_0 \varepsilon_0 \varepsilon_r Df \quad (10)$$

In order to verify the validity of (9) for representing the dielectric losses considering the structure and dimensions of the SIWs that will be used in the experimental part of this research, the SIW described in Fig. 5 was simulated in HFSS assuming $Dk = 2.2$ and $Df = 0.0009$ for the substrate, and perfect conductors. As can be seen in Fig. 6, excellent agreement is observed between the attenuation obtained from the simulations and that calculated using (9). This indicates the adequateness of the analytical model for the dielectric attenuation.

Conductor Losses

The conductor losses, associated with the finite conductance of the metals defining the structure of a SIW are quantified through α_c . This attenuation component can be obtained from a ratio involving the power loss per unit length in the conductor material (P_l) and the power flow down the SIW assuming no losses occurring in the dielectric (P_f). The corresponding expression is [13]:

$$\alpha_c = \frac{P_l}{2P_f} \quad (11)$$

where P_f depends on the width and the thickness of the waveguide, whereas P_l includes the contribution of the losses occurring on the top and bottom planes (which depend on w_{eff}), and the losses in the side walls (which are dependent on t). In fact, the total conductor attenuation can be expressed as the sum of the attenuation components

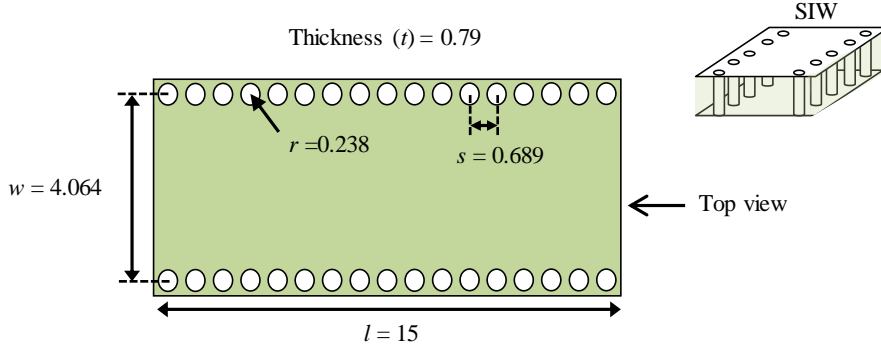


Figure 5: Structure simulated using a full-wave solver to verify the validity of the loss models (units are in mm).

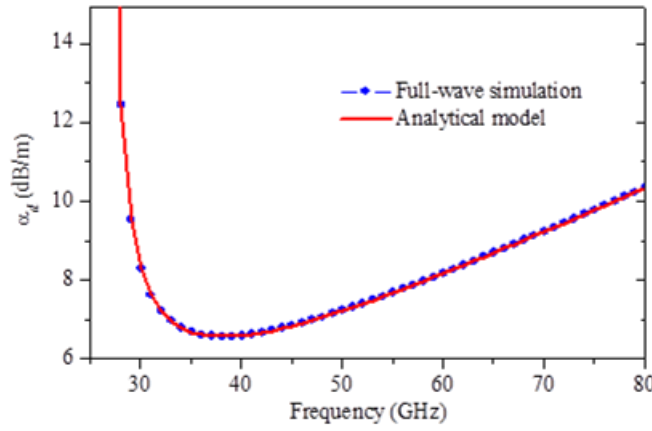


Figure 6: Comparison between α_d obtained from simulations and applying (9).

associated with the losses in the top and bottom planes (α_{tb}) and those in the side walls (α_{tb}):

$$\alpha_c = \alpha_{tb} + \alpha_{sw} \quad (12)$$

Each term of this mathematical expression is promptly explained.

Attenuation Due to Losses on Top and Bottom Metal Layers

The expression that represents this attenuation component for the mode TE_{10} is [13]:

$$\alpha_{tb} = \frac{2\pi R_s \epsilon_0 \epsilon_r}{\beta t} f \quad (13)$$

where R_s is the surface resistance of the metal layer; due to the skin effect, this resistance depends on frequency and can be expressed as follows:

$$R_s = C_s \sqrt{f} \quad (14)$$

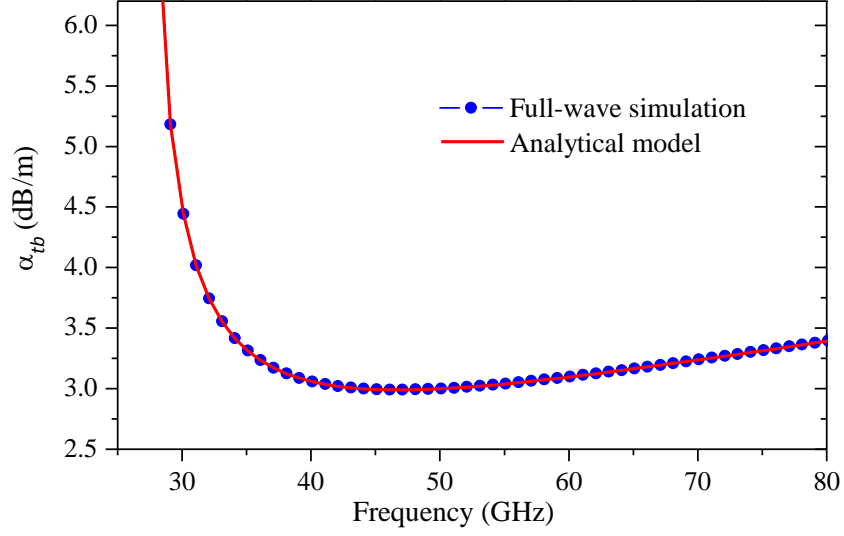


Figure 7: Comparison between α_{tb} obtained from simulations and applying (15).

where C_s is a proportionality constant. Thus, (13) can be rewritten as:

$$\alpha_{tb} = \left(\frac{k_2 f^{1.5}}{t} \right) \beta^{-1} \quad (15)$$

with:

$$k_2 = 2\pi C_s \varepsilon_0 \varepsilon_r \quad (16)$$

In contrast with the coefficient k_1 in (9) for the dielectric attenuation, which is only related to the properties of the dielectric, the factors relating the conductor attenuation components with frequency are affected by the geometry of the SIW [i.e. k_2/t in (15)]. For instance, notice that according to (15) the product $\alpha_{tb}\beta$ is inversely proportional to t and is not affected by w_{eff} . This independence of $\alpha_{tb}\beta$ to the SIW width occurs because a change in w_{eff} changes P_l and P_f (i.e., the losses increase in the top and bottom layers but also the capacity of the guide to handle power). Conversely, when the SIW thickness changes, only P_f is affected. Thus, thinning the SIW considering a constant width would reduce P_f while P_l remains constant, which increases $\alpha_{tb}\beta$ as predicted by (11).

In order to verify the model accuracy, the SIW described in Fig. 5 was simulated using HFSS considering perfect non-lossy dielectric and perfect conductor for the side walls. For the top and bottom planes, copper was defined. Fig. 7 shows the confrontation of the attenuation curves obtained from the simulation and by applying the model given by (15). Excellent correlation is observed.

Impact of Surface Roughness on Conductor Losses

Although (15) shows accuracy, the results in Fig. 7 correspond to perfectly smooth metal layers. Nonetheless, due to the rough metal foils used in current PCB manufacturing technology, validating the model for α_{tb} considering this imperfect condition is necessary.

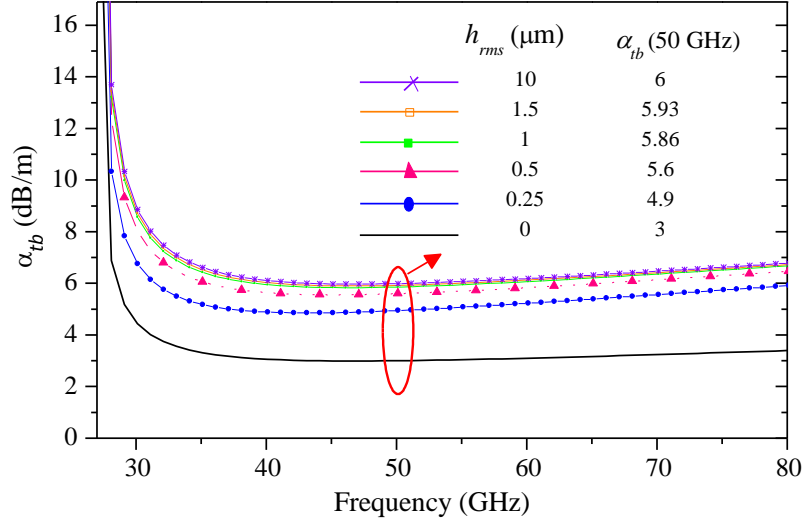


Figure 8: Attenuation due to the top and bottom metallic layers for different h_{rms} values.

In this regard, the metal surface roughness is typically quantified using the mean-square-root of the protuberances (h_{rms}), which takes values in the order of a few micrometers [14]. It is worthwhile pointing out that the importance of taking the effect of the surface roughness into account relies on the fact that, the skin depth (δ) is comparable with h_{rms} at microwave frequencies. This causes an increment in the attenuation attributed to the conductor losses. In fact, typical approaches consider this effect for quasi-TEM transmission lines by assuming that a trace with rough surface profile presents the resistance as if smooth metal is used but multiplied by a frequency-dependent coefficient (K_H) explained in [15]. We have experimentally observed that the same concept applies for SIWs when considering that R_s , as defined in (14), is the resistance affected by this same term.

Once again, the structure of Fig. 5 was simulated. Now, perfect dielectric for the substrate and perfect conductor for the side walls were defined; this time, however, in addition to considering that the top and bottom layers are made of copper, different values of h_{rms} were defined for the inner faces of these layers in the course of several simulations. Fig. 8 shows the results corresponding to α_{tb} for six different values of h_{rms} ; as can be observed, a considerable increase in the attenuation is exhibited by the SIW presenting $h_{rms} = 0.25 \mu\text{m}$ when compared with that assuming smooth metal layers. In fact, the increase in the attenuation remains gradual as h_{rms} rises, although it is barely noticeable within the considered frequency range for $h_{rms} > 1.5$. In fact, it is possible to see that α_{tb} for the extreme considered case ($h_{rms} = 10 \mu\text{m}$) approximately doubles that corresponding to the SIW with the smooth layers beyond 50 GHz, which is analyzed below.

Now, it is time to incorporate the effect of the surface roughness into the SIW model for α_{tb} ; the straightforward way modifies (15) to yield:

$$\alpha_{tb} = K_H \left(\frac{k_2 f^{1.5}}{t} \right) \beta^{-1} \quad (17)$$

where K_H is defined as in [15] and requires previous knowledge of h_{rms} for a particular prototype. Bear in mind, however, that from an experimental point of view, it is desirable to implement the model directly from S -parameters without involving additional measurements. In this case, implementing (17) would be complicated considering that K_H is frequency dependent and also the experimental data would include other effects. For this reason, an alternative model is proposed here for accurately representing the metal losses including the effect of the surface roughness; this is expressed as:

$$\alpha_{tb} = \left(\frac{k_2 f^{1.5}}{t} + k_3 \right) \beta^{-1} \quad (18)$$

where k_2 and k_3 are parameters that depend on h_{rms} but not on frequency. Fig. 9 shows the good agreement between (18) and full-wave simulations. Moreover, k_2 shows an interesting trend when plotted versus h_{rms} . Notice in Fig. 10 that the value for this parameter for rough metal layers doubles that corresponding to smooth ones. On the other hand, at this stage, k_3 is only used for fitting purposes.

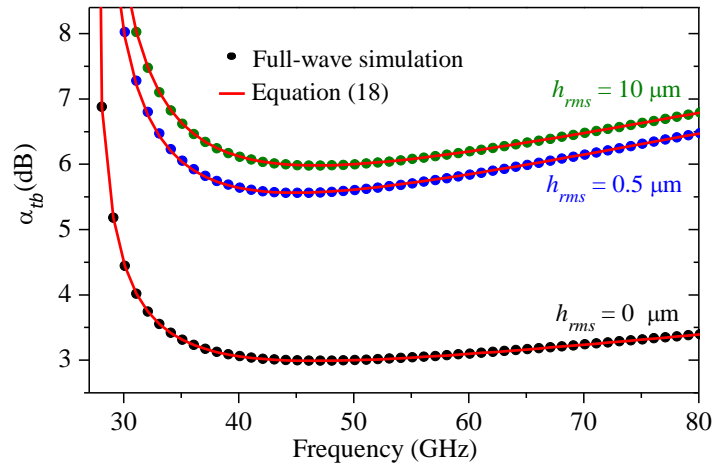


Figure 9: Comparison between α_{tb} obtained from simulations and applying (18) considering different h_{rms} values (values in μm).

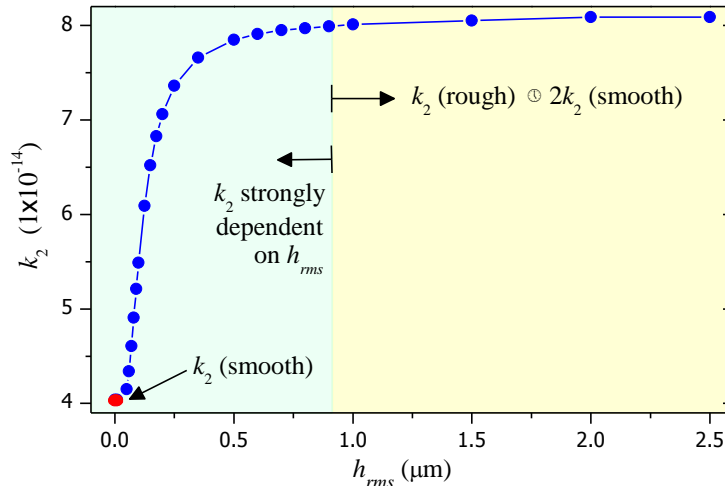


Figure 10: Values of k_2 for different roughness.

Attenuation Due to Losses on the Side Walls

The conductor losses on the side walls also introduce attenuation. According to [13], the attenuation related to these losses (α_{sw}) can be calculated as:

$$\alpha_{sw} = \frac{k_4}{\beta} f^{-0.5} \quad (19)$$

where:

$$k_4 = \frac{2\pi C_s}{\mu_0 w_{eff}^3} \quad (20)$$

It is interesting to observe that considering (19), (20) and the mode of propagation TE_{10} (for which β depends on w_{eff}), the product $\alpha_{sw}\beta$ depends on w_{eff} and is not influenced by t . This dependence is explained in the same way as the relation between $\alpha_{tb}\beta$ and t . In this case, considering a fixed SIW thickness, reducing w_{eff} causes that P_f is lowered while P_l remains constant. Therefore, as dictated by (11), α_{sw} increases as the width of the waveguide is reduced. On the other hand, changing the thickness of the SIW while maintaining constant the width modifies P_f and P_l in the same proportion, which yields no change in the value of α_{sw} .

With the purpose of verifying the validity of (19) for the SIWs used in this work, the structure shown in Fig. 5 was simulated in HFSS, but now assuming that the vias forming the side walls are made of copper. To analyze this particular effect, perfect dielectric for the substrate and perfect conductor for the top and bottom planes were defined. Fig. 11 shows the confrontation of α_{sw} obtained using (19) with the simulated results. An excellent correlation is observed, where α_{sw} monotonically decreases with frequency.

Experimental results shown later in this paper point out that the effect of α_{sw} is small for SIWs in standard PCB technology [16]. Thus, for practical purposes α_c can be

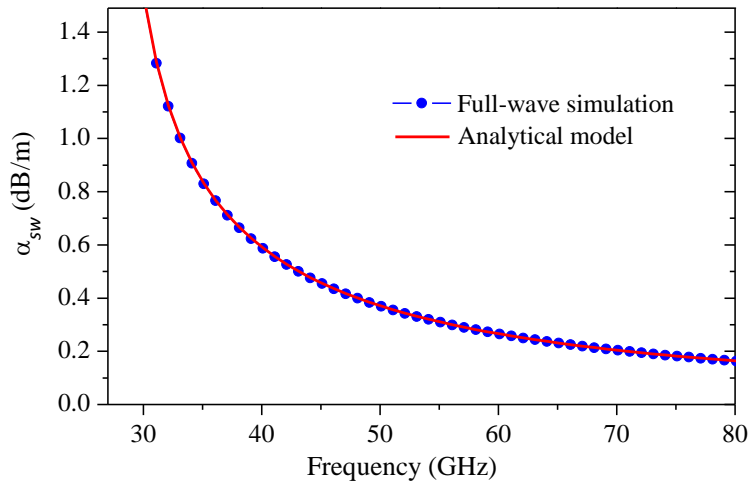


Figure 11: Comparison between α_{sw} obtained from simulations and applying (19).

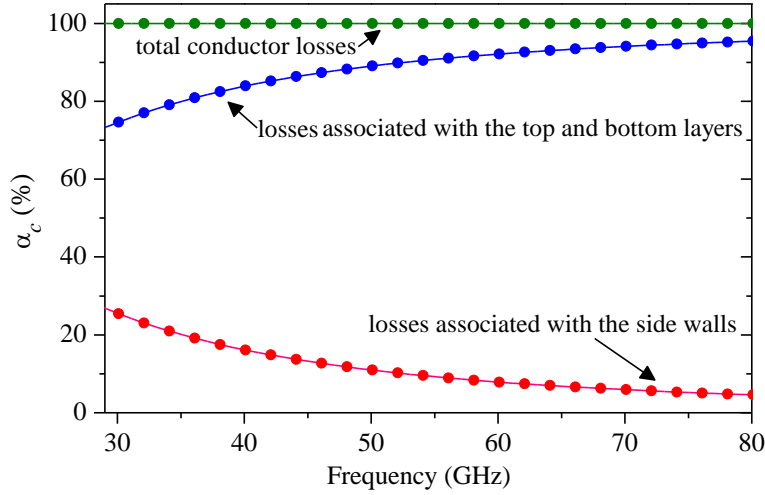


Figure 12: Contribution of top and bottom layers attenuation and side walls attenuation in the total conductor attenuation.

approximated to α_{tb} . Fig. 12 shows the percentage of the separate contribution of α_{sw} and α_{tb} to the total conductor attenuation. As the reader infers, this assumption has to be checked for particular geometries when the research interest is on the characterization of the metal properties. In fact, it is shown latter that an additional reason for assuming α_{sw} as negligible is because $\alpha_{sw} \ll \alpha_{tb} + \alpha_d$.

Model for the Total Attenuation

In previous sections, the models for dielectric and conductor attenuation components have been described and verified through full-wave simulations. In order to identify the contribution of every type of loss to the total attenuation for the structure defined in Fig. 5, the corresponding curves are plotted in Fig. 13. As can be seen, more than 50% of the losses are related to the dielectric, while the attenuation related to the side walls accounts for less than 10% for frequencies higher than 30 GHz. Thus, neglecting α_{sw} , we can

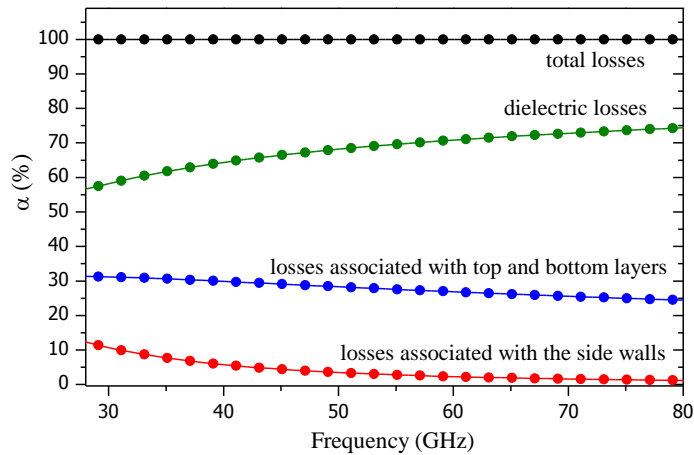


Figure 13: Contribution of the different types of loss to the total SIW attenuation. Smooth metal planes are considered.

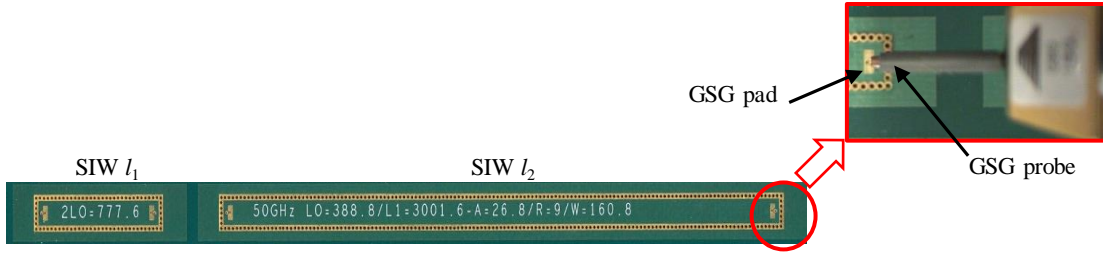


Figure 14: Photographs of two of the fabricated SIWs.

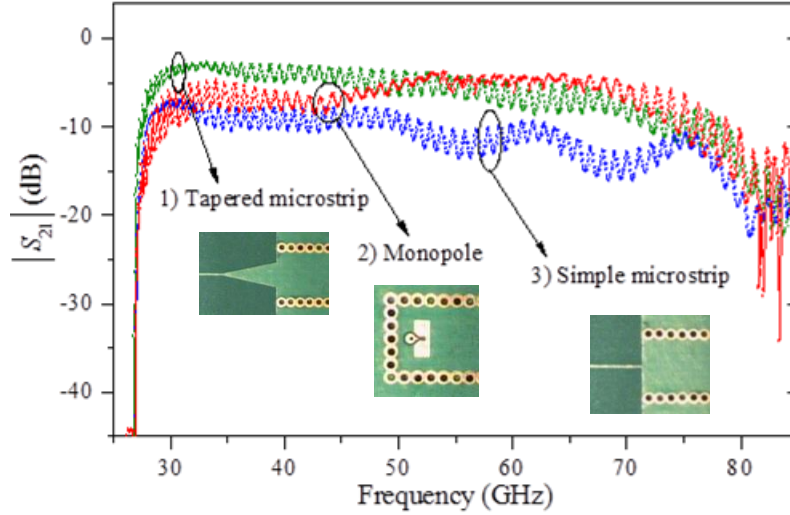


Figure 15: Experimental insertion loss for SIWs presenting different signal launchers.

combine the models for α_d and α_{tb} in order to obtain an expression that represents the total attenuation in a SIW:

$$\alpha_{total} = \left(k_1 f^2 + \frac{k_2}{t} f^{1.5} + k_3 \right) \beta^{-1} \quad (21)$$

In the following sections, this model is used to represent the attenuation obtained from measurements of SIWs presenting different geometries.

3 Experimental Results

In order to experimentally verify the model discussed in previous sections, SIWs were fabricated on PCB in a dielectric substrate with nominal Dk and Df of 2.2 and 0.0017, respectively. Metal layers of 1 oz of copper and presenting VLP surface were used. The dimensions and spacing between the vias forming the side walls correspond to those shown in Fig. 5. The SIWs were fabricated for different widths ($w = 4.1$ mm, 2.3 mm, and 1.8 mm), lengths ($l = 76$ mm and 254 mm), and in substrates with two different thicknesses ($t = 0.127$ mm and 1.4 mm). Fig. 14 shows two of the fabricated SIWs and the detail of the pads for probing.

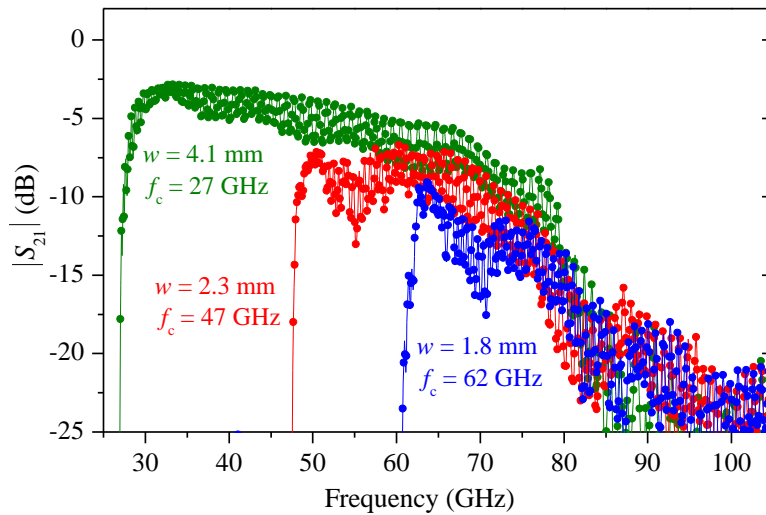


Figure 16: Experimental insertion loss for SIWs with different width and fixed length ($l = 76$ mm).

S -parameter measurements were performed to these SIWs at frequencies up to 110 GHz by using a vector network analyzer (VNA) and coplanar RF microprobes. For this purpose, the VNA setup was calibrated up to the probe tips by using an LRRM algorithm and an impedance-standard-substrate (ISS). After S -parameters were measured, the propagation constant ($\gamma = \alpha + j\beta$) was determined using a line-line method so that the total attenuation per-unit-length could be obtained [17]. In this case, two SIWs varying only in length were used to obtain γ for every combination of width and substrate thickness.

In order to experimentally determine the most appropriate transition to excite the SIWs, different types of launch structures were implemented and measured. Fig. 15 presents the insertion loss for three types of launchers: 1) tapered microstrip, 2) monopole, and 3) simple microstrip. Due to diminished reflections and better transmission properties, the selected SIWs for performing our analysis were those presenting the tapered microstrip launchers. The experimental insertion loss for three SIWs presenting this transition are plotted in Fig. 16. Detailed rules for designing the taper can be found in the literature [18].

Model-Experiment Correlations

This section is dedicated to show the implementation of the model given by (21) to represent the characteristics of the fabricated SIWs. As mentioned when detailing the fabricated prototypes, different widths and dielectric thicknesses are studied in order to observe how the different components of the total attenuation change. Thus, in order to keep the explanation corresponding to each structure organized, the main characteristics of the SIWs modeled are summarized in Table 2, where reference numbers are assigned to each case.

Number of SIW (reference)	Width (mm)	Cutoff frequency (GHz)	Thickness (mm)
SIW-1	4.1	27	1.4
SIW-2	4.1	27	0.127
SIW-3	2.3	47	1.4
SIW-4	1.8	62	0.127

Table 2: Characteristics of the fabricated SIW.

Number of SIW (reference)	k_1	k_2/t
SIW-1	8.78×10^{-19}	4.59×10^{-14}
SIW-2	8.78×10^{-19}	5.05×10^{-13}
SIW-3	8.68×10^{-19}	4.41×10^{-14}
SIW-4	8.71×10^{-19}	5.3×10^{-13}

Table 3: Values for the model parameters for the considered SIWs.

Equation (21) was implemented through parameter optimization to represent the attenuation for every case detailed in Table 2, which yields the values listed in Table 3. As expected, constant values for these parameters allow a proper representation of the experimental data as verified in Fig. 17, which shows the experimental and modeled total attenuation obtained for every waveguide analyzed. Notice the excellent model-experiment correlation observed in every case, even for the noisy data corresponding to

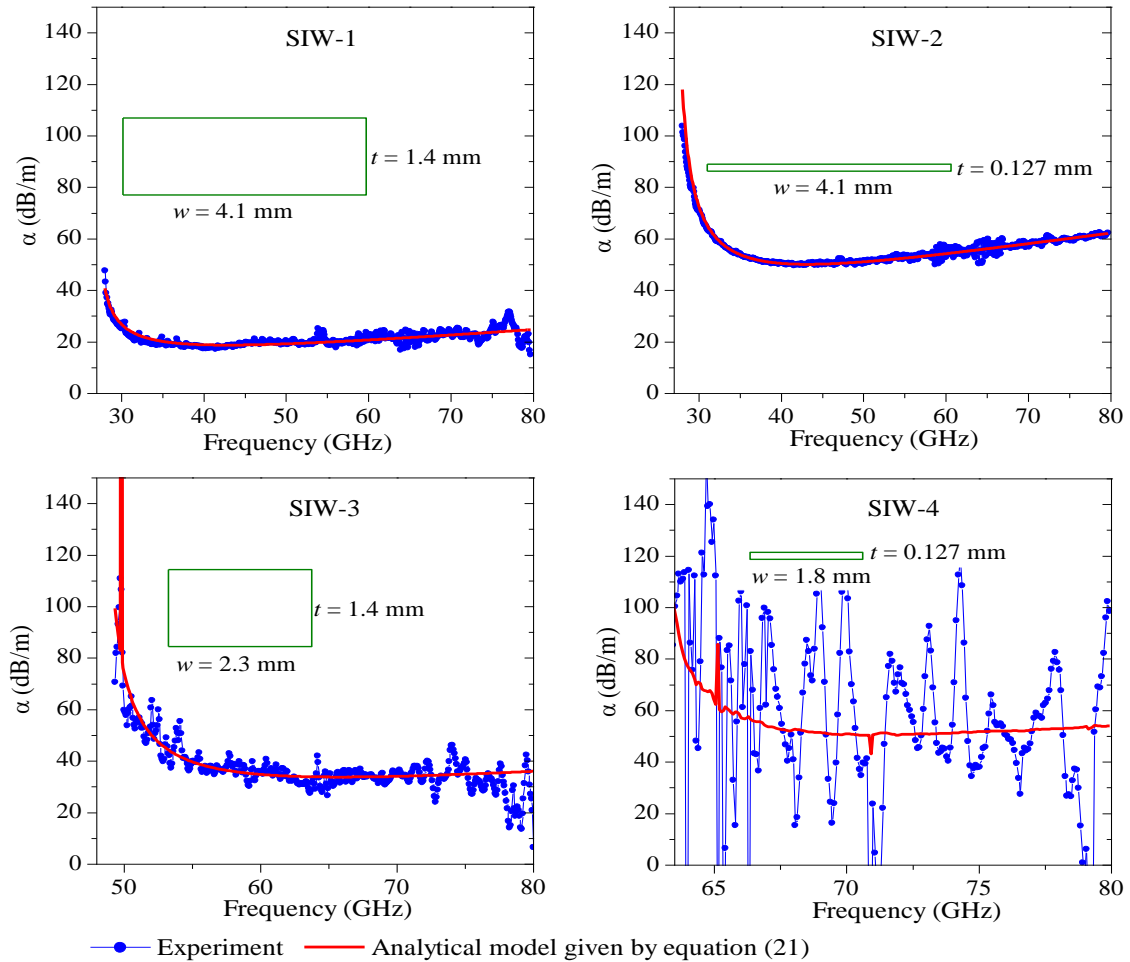


Figure 17: Comparison between the experimental attenuation and the proposed model. Notice that the fluctuations observed in the curve corresponding to the model for the case (4) are due to the fact that the experimental β is used in (21), which is noisy for the SIW with the smallest cross section.

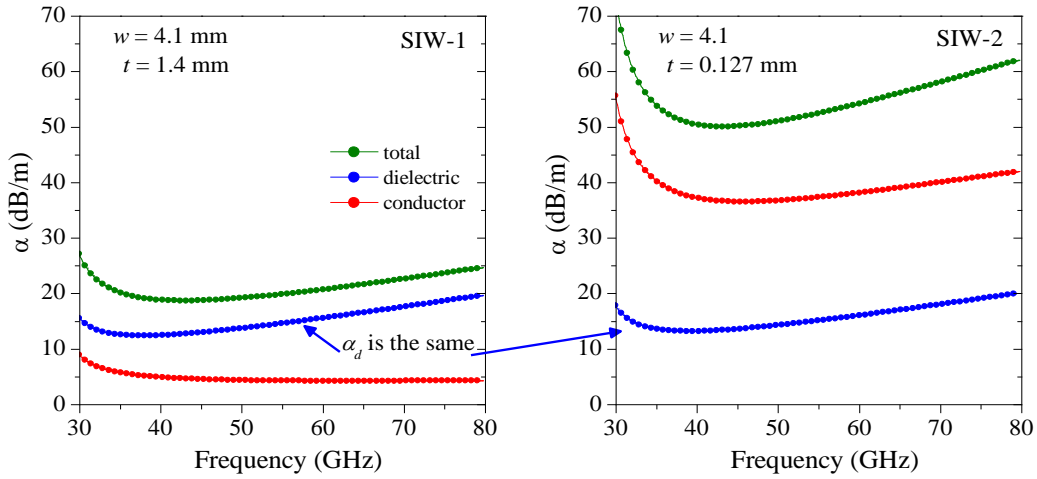


Figure 18: Simulated total, dielectric, and conductor attenuation of two SIWs with different dielectric thickness. The curves are obtained after correlating (21) with experimental data.

the narrowest SIW [SIW-4 in Fig. 17], which presents the smallest cross section and consequently is capable of handling less power. Unfortunately, this diminished power capability introduces a high uncertainty in the determination of α and β from the experimental S -parameters.

The model-experiment correlations shown in Fig. 17 also allow to observe that, as theoretically expected, the attenuation in a SIW is inversely proportional to both the width (e.g. compare SIW-1 and SIW-3), and the dielectric thickness (compare SIW-1 and SIW-2). While comparing the curves, however, consider the different cutoff frequencies.

An important point to be remarked is the physically-expected variation of k_2/t listed in Table 3: from Table 2, it can be noticed that the thickness of SIW-1 is eleven times larger than the thickness of SIW-2 and both present the same geometric width. Accordingly, k_2/t is eleven times larger for SIW-2 than for SIW-1. This points out the validity of the model proposed for α_{tb} , which predicts that the attenuation related with the top and bottom planes of the SIW even when incorporating the effect of the metal surface roughness. Moreover, for structures presenting the same thickness and only changing in width, the value of k_2/t is very similar because as we know, k_2 does not depend on w_{eff} .

In order to analyze the importance of the substrate thickness in the losses of the SIW, the attenuation curves for two SIWs with fixed w and different t are plotted in Fig. 18. Since both SIWs present the same cutoff frequency and propagate in the TE_{10} mode, both exhibit the same β versus frequency curves and thus, the same level for the dielectric attenuation. Therefore, the increment in the total attenuation of the SIW as reducing t is due to an increment of the losses associated with the conductor. This effect can be inferred when comparing the curves shown in Fig. 18: the curves corresponding to α_d for both structures are approximately the same while α_c is substantially different. In fact, α_c increases as t is reduced because of the corresponding increase in attenuation due to the top and bottom layers. This is the reason why the total attenuation curve in the plot at the right-hand of Fig. 18 is much higher than for the other case.

The discussion in the previous paragraph is fundamental when selecting the optimum prototype for characterizing the dielectric characteristics of a PCB substrate from measurements performed to SIWs: selecting a thick and wide SIW allows for minimizing the conductor losses in order to achieve a better extraction of the dielectric characteristics from the experimental attenuation. In any case, provided that the appropriate model is considered to represent the SIW, Dk and Df can be obtained as long as the signal-to-noise ratio of the measurements do not considerably penalize the parameter extraction certainty.

Determination of Dielectric Parameters

In order to obtain the characteristics of the PCB dielectric, knowing the separate contribution of the conductor and dielectric losses is required. For this purpose, equation (21) is written for SIWs with different geometries (e.g. SIW-1 and SIW-2). Afterwards, the resulting equations are simultaneously solved to determine the parameters for the conductor attenuation model: k_2 (which remains constant with geometry) and k_3 (which is dependent on the SIW's width and thickness). At this point, α_c is known for the two SIWs used in the described parameter extraction; thus, α_d can be obtained as a function of frequency by performing a subtraction $\alpha_d = \alpha - \alpha_c$ involving the experimental data corresponding to any of these SIWs. It is worthwhile to mention that, in order to experimentally obtain Dk and Df , measurements performed on SIW-1 ($w = 4.1$ mm, $t = 1.4$ mm) were used at this stage since the conductor losses are low (see Fig. 18) and potential errors in the modeled curve for α_c hardly impact α_d . However, during our analysis, even processing data corresponding to other of the fabricated structures (e.g. SIW-2) allowed to obtain the dielectric parameters in a consistent manner.

To finalize the parameter extraction, Dk was obtained by means of equation (7), which is straightforward since all the required parameters are known. Afterwards, the imaginary part of the permittivity was obtained from (8) and considering only the dielectric attenuation; therein lies the utility of the model for the attenuation. With the real and imaginary part of the permittivity defined, Df could be obtained by using (6). The results are shown in Fig. 19.

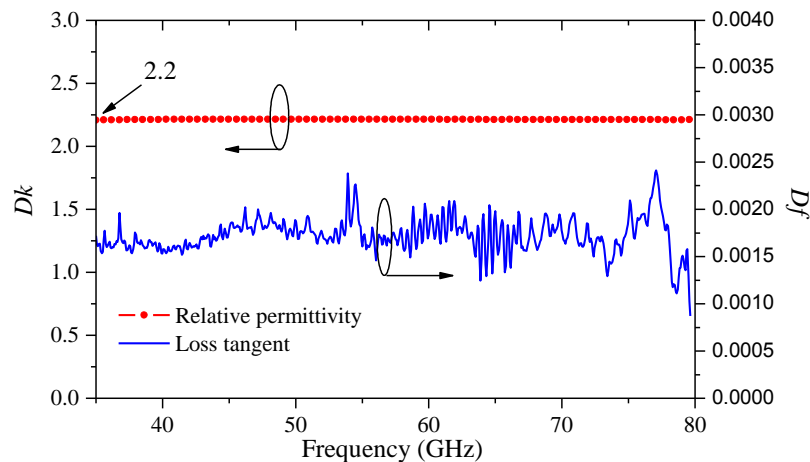


Figure 19: Experimentally obtained Dk and Df .

Advantages of Exciting Higher-Order TE₂₀ Mode

Nowadays, the knowledge of dielectric properties of substrates in-situ is required at high frequencies even within the W-band. In this regard, the method proposed here can be applied with this purpose, and the obvious solution to achieve higher frequencies is building prototype SIWs with higher cutoff frequencies. However, the increment in the cutoff frequency implies a reduction in the size of the waveguide. Unfortunately, as we discussed in previous sections, shrinking the waveguides makes the conductor losses considerably much larger than the dielectric losses. Therefore, the uncertainty of the characterization technique increases accordingly. In order to be more specific, notice that the SIW presenting the smallest cross section in Fig. 17 (i.e. SIW-4) is capable of handling less power than any other among the implemented prototypes. The main inconvenience of this structure is that the diminished cross section required to extend the monomode operation to higher frequencies is also accompanied by a less power flow while the attenuation increases (compare SIW-1 and SIW-3 in Fig. 17). In this section, an alternative to be explored to enable the proposed method for application at higher frequencies without reducing the size of the SIWs is discussed.

Let us start by emphasizing that SIWs can transmit different propagation modes, but only the excited mode with smallest cutoff frequency allows the propagation of EM waves in single mode. For instance, if TE₁₀ mode is excited by applying the stimulus right in the middle of the SIW, monomode operation occurs until the cutoff frequency of the TE₃₀ is reached; beyond this frequency both modes will be propagated until the cutoff frequency of the TE₅₀ mode is also reached (this process continues for higher-order odd modes). Notice in this case, that the TE₂₀ mode is not excited due to the point where the stimulus was applied. In fact, to excite the TE₂₀ mode it is necessary to apply the stimulus at two different points with a difference in phase of 180°. Why exciting this mode would be interesting? This is explained afterwards.

First, we establish that there exists a relation between the cutoff frequency of the TE₁₀ and TE₂₀ modes given by $f_c(\text{TE}_{20}) = 2f_c(\text{TE}_{10})$. Therefore, when the stimulus of a SIW makes the TE₂₀ mode the fundamental operation mode, monomode operation can be extended to higher frequencies for any SIW of a given width. See for instance in Fig. 20, a SIW operating in the TE₂₀ mode is twice as wide and presents lower attenuation than a SIW designed to operate in the TE₁₀ within the same frequency range. According to this, the characterization of dielectrics using SIWs operating in the TE₂₀ offers significant advantages. However, the challenge in this case is designing the appropriate excitation configuration for the SIW. Four-port VNA setups can be used, but placing either the connector or probing interfaces is more complicated. Alternatively, different structures that allow the propagation of the TE₂₀ mode in SIWs have been reported using one point of stimulus application [19]. These structures are based on the concept of stimulus application at both sides of the SIW [20], and this work will comprise the topic of our follow-up investigations which are currently ongoing.

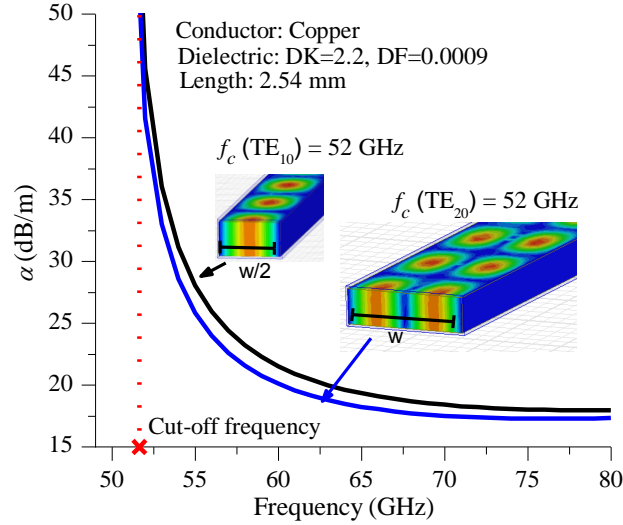


Figure 20: Comparison between SIWs with the same f_c and different mode of propagation (TE_{10} and TE_{20}).

Conclusions

The potential of SIWs to accurately characterize dielectric properties was presented. The critical importance of representing losses associated with the conductors forming the structure (since their impact is substantial at tens of gigahertz) was also addressed. To implement this robust characterization, an accurate model that even considers the effect of the metal surface roughness was proposed and verified through intensive simulations and model-experiment data correlations. In order to show the scalability of the proposed model, our analysis included the processing of data corresponding to SIWs configured with varying dimensions and operating at different frequencies, thereby showing consistency and expected geometry-dependent trends of the associated parameters. Ultimately, using this model, obtaining Dk and Df of PCB materials at millimeter-wave frequencies was shown using a simple extraction procedure.

References

- [1] H. Kassem, V. Vigneras, G. Lunet, "Characterization techniques for materials' properties measurement" in *Microwave and Millimeter Wave Technologies: from Photonic Bandgap Devices to Antenna and Applications*, InTech, 2010, pp. 289-314.
- [2] L. Chen, C. Ong and B. T. G. Tan, "Amendment of cavity perturbation method for permittivity measurement of extremely low-loss dielectrics", *IEEE Trans. Instrum. Meas.*, vol. 48, no. 6, pp.1031 -1037 1999.
- [3] K. Saeed, R. D. Pollard, and I. C. Hunter, "Substrate integrated waveguide cavity resonators for complex permittivity characterization of materials", *IEEE Trans. Microw. Theory Tech.*, vol. 56, no. 10, pp. 2340–2347, 2008.
- [4] J. Simpson, A. Taflove, J. Mix and H. Heck, "Substrate integrated waveguides optimized for ultrahigh-speed digital interconnects", *IEEE Trans. Microw. Theory Tech.*, vol. 54, no. 5, pp.1983 -1990 2006.

- [5] G. Romo and A. Ciccomancini, "Substrate integrated waveguide (SIW) filter: Design methodology and performance study", Proc. IEEE MTT-S IMW Symp., pp.23 -23 2009.
- [6] D. Deslandes, and K. Wu, "Design consideration and performance analysis of substrate integrated waveguide components," 32nd European Microwave Conference Proceedings, vol. 2, pp. 881-884, September 2002.
- [7] J. E. Rayas-Sanchez and V. Gutierrez-Ayala, "A general EM-based design procedure for single-layer substrate integrated waveguide interconnects with microstrip transitions," in Microwave Symposium Digest, 2008 IEEE MTT-S International, pp. 983-986, 2008.
- [8] R. Torres-Torres, G. Romo, B. Horine, A. Sánchez and H. Heck, "Full Characterization of Substrate Integrated Waveguides from S-Parameter Measurements", in Proc. IEEE EPEPS Conf., pp. 277–280, 2006.
- [9] Bozzi, M., Pasian, M., Perregrini, L., Wu, K.: "On the losses in substrate integrated waveguides and cavities", Int. J. Microw. Wirel. Technol., 1, (5), pp. 395 –401, 2009.
- [10] K. Wu, D. Deslandes, Y. Cassivi, "The substrate integrated circuits - a new concept for high-frequency electronics and optoelectronics", TELSIKS'03, pp. P-III – P-X, Nis, Yugoslavia, Oct. 2003.
- [11] <http://www.microwaves101.com/encyclopedias/microwave-rules-of-thumb>.
- [12] M. D. Janezic, J. A. Jargon, "Complex permittivity determination from propagation constant measurements", IEEE Transactions on microwave theory and techniques, vol. 42, no. 2, 1994.
- [13] D. M. Pozar, Microwave Engineering, Ed. Wiley, 2005.
- [14] S. Hall and H. Heck, Advanced Signal Integrity for High-Speed Digital Designs, Ed. New Jersey: Wiley-IEEE Press, 2009.
- [15] E. Hammerstad and O. Jensen, "Accurate models of computer aided microstrip design", IEEE MTT-S Symposium Digest, pp. 407–409, 1980.
- [16] X. C. Zhu, W. Hong, K. Wu, K.-D. Wang, L.-S Li, Z.-C. Hao, H.-J. Tang and J.-X. Chen, "Accurate characterization of attenuation constants of substrate integrated waveguide using resonator method", IEEE Microw. Wireless Compon. Lett., vol. 23, no. 12, pp.677 -679, 2013.
- [17] J.A. Reynoso-Hernández, "Unified method for determining the complex propagation constant of reflecting and nonreflecting transmission lines", IEEE Microwave Wireless Comp. Lett., Vol. 13, pp. 351–353, 2003.
- [18] D. Deslandes, "Design equations for tapered microstrip-to substrate integrated waveguide transitions", IEEE MTT-S Int. Microw. Symp. Dig., pp.704 -707 2010.
- [19] P. Wu, J. Liu and Q. Xue, "Wideband Excitation Technology of TE₂₀ Mode Substrate Integrated Waveguide (SIW) and Its Applications", IEEE Trans. Microw. Theory Tech., vol. 63, no. 6, pp. 1863–1874, 2015.
- [20] Z.-Y. Zhang and K. Wu, "A broadband substrate integrated waveguide (SIW) planar balun", IEEE Microw. Wireless Compon. Lett., vol. 17, no. 12, pp.843 -845 2007.